17 Shannon MF, Coles LS, Fielke RK, Goodall GJ, Lagnado CA, Vadas MA. Three essential promoter elements mediate tumour necrosis factor and interleukin-1 activation of the granulocyte-colony stimulating factor gene. *Growth Factors* 1992; **7**: 181–93.
18 Tachibana M, Miyakawa A, Tazaki H *et al.* Autocrine growth of transitional cell carcinoma of the bladder induced by granulocyte-colony stimulating factor. *Cancer Res* 1995; **55**: 3438–43.
19 Hirata T, Shimazaki C, Sumikuma T *et al.* Humanized anti-interleukin-6 receptor monoclonal antibody induced apoptosis of fresh and cloned human myeloma cells in vitro. *Leuk Res* 2003; **27**: 343–9.
20 Coward J, Kulbe H, Chakravarty P *et al.* Interleukin-6 as a therapeutic target in human ovarian cancer. *Clin Cancer Res* 2011; **17**: 6083–96.

Original Investigations

Pleural Invasion by Peripheral Lung Cancer:

Prediction with Three-Dimensional CT

Kiyonori Ebara, Shodayu Takashima, MD, PhD, Binghu Jiang, MD, Hodaka Numasaki, PhD, Mai Fujino, Yasuhiko Tomita, MD, Katsuyuki Nakanishi, MD, Masahiko Higashiyama, MD

Rationale and Objectives: To evaluate the clinical utility of three-dimensional (3D) computed tomography (CT) for predicting pleural invasion by peripheral lung cancer.

Materials and Methods: CT findings (tumor size, vertical diameter, length and area of the interface between tumor and the pleura, ratios of length and area [R_{area}] of interface between tumor and the pleura to tumor size, angle between the tumor and adjacent pleura, presence or absence of pleural thickening, and originally developed 3D pleural patterns) in 201 consecutive patients with lung cancer of ≤3 cm in contact with pleural surface were correlated with pathologic findings. Logistic modeling was used for determining the significant factors for prediction of pleural invasion, and receiver operating characteristic (ROC) curves were used for investigating diagnostic capability of significant factors, resulting in a recommendation to the optimal criteria for predicting pleural invasion and to the optimal threshold for differentiating parietal from visceral invasion.

Results: Sixty-one (30%) of the 201 patients had pathologically verified pleural invasion. Logistic modeling revealed that the 3D pleural pattern was the only significant factor ($P < .001$; relative risk of 7.34). Among every combination of the 3D patterns, skirt-like pattern showed the highest accuracy of 77% for predicting pleural invasion. In differentiating parietal from visceral pleural invasion, ROC analysis revealed that R_{area} was optimal for differentiating parietal from visceral pleural invasion, and the highest accuracy of 77% was obtained with a cut-off value of 13.4 for this criterion.

Conclusions: Computer-aided 3D CT analysis of the pleura was useful for predicting pleural invasion.

Key Words: 3D CT; pleural invasion; lung cancer; computer-aided diagnosis.

The anatomic extent of disease as expressed by the tumor, node, and metastasis staging system is the most important prognostic factor for lung cancer. Presence of visceral pleural invasion by lung cancer increases T staging from T1 to T2, and the presence of parietal pleural invasion upstages it from T2 to T3, when the tumor is <3 cm in size (1). Therefore, prognosis of patients with T1-sized (≤3 cm) lung cancer depends on the presence or absence of pleural invasion and the depth of invasion of the pleura (2). Five-year survival rates are reported to worsen from 86% (for patients with no pleural invasion) to 62%–70% (for patients with visceral pleural invasion) and then to 57% (for patients with parietal pleural invasion) for non–small cell lung cancer (NSCLC) (3).

Computed tomography (CT) is currently the imaging method of choice in staging of lung cancer. However, a well-known limitation of conventional CT is the diagnosis of pleural invasion by peripheral lung cancer. Sensitivity in diagnosing invasion of the parietal pleura or chest wall based on two-dimensional (2D) CT is reported to range from 38% to 89.7% and specificity from 40% to 96% (4,5). However, the visceral pleural invasion is difficult to diagnose with CT and has not been assessed in detail, especially in patients with T1-sized lung cancer. Thin-section spiral CT allows continuous data collection and provides uninterrupted volume data that can be reconstructed to produce three-dimensional (3D) images, which have been reported to be superior to 2D CT in the assessment of pleural invasion by lung cancer (6).

The objective of this study was to evaluate the value of 3D CT in diagnosing pleural invasion and differentiating parietal from visceral pleural invasion by T1-sized peripheral lung cancer.

Acad Radiol 2014; ■:1–10

From the Department of Functional Diagnostic Science, Osaka University Graduate School of Medicine, 1-7 Yamadaoka, Suita, Osaka 565-0871, Japan (K.E., S.T., B.J., H.N., M.F.); and Osaka Medical Center for Cancer and Cardiovascular Diseases, Higashinari-ku, Osaka, Japan (Y.T., K.N., M.H.). Received June 3, 2014; accepted October 8, 2014. **Address correspondence to:** K.E. e-mail: kiyoharu0825@yahoo.co.jp

http://dx.doi.org/10.1016/j.acra.2014.10.002

MATERIALS AND METHODS

This retrospective study was approved by our institutional review board and written informed consent was obtained from all participants for the use of thin-section CT data.

Patients

Between January 2007 and December 2012, 1003 patients with peripheral lung cancer of ≤3 cm underwent thin-section CT examinations before surgery and subsequent surgical resection of lung cancer. Of these, 422 tumors in 422 patients and 380 tumors in 380 patients were excluded from the present study because the former tumors were remote from the pleura and had no pleural tag on thin-section CT images (lung window setting), and the latter ones were also remote from the pleura but had pleural tags only. A pleural tag was defined as a linear strand originating from the nodule surface and reaching the pleural surface. Thus, 201 consecutive patients (126 men and 75 women; age, 66.7years ± 9.3 [mean ± standard deviation, SD]) with tumors in contact with pleura were included in this series. In our institute, the following nodules were recommended surgical resection with or without preceding biopsy procedures (depending on the size of the nodules): mixed ground-glass opacity nodules of ≥5 mm that are stable in size or show interim growth; solid nodules of ≥5 mm that show interim growth. The median interval time between thin-section CT and surgery was 14 days (range, 1–30 days).

Thin-Section CT

A 16-slice CT scanner (Aquilion 16; Toshiba, Tokyo, Japan) was performed during a single breath hold with (n = 153) or without (n = 48) intravenous contrast agent. Technical parameters of CT scans were 120 kVp, 100–150 mA, 0.5 s/rotation, and 16 × 0.5 mm collimation. Axial images of 1.0 mm thickness with 0.5 mm spacing were reconstructed with a matrix of 512 × 512 and a field of view of 350 × 350 mm. The spatial resolution for reconstruction images was 0.7, 0.7, and 1.0 mm on x-axis, y-axis, and z-axis, respectively. The conventional 2D CT images and the 3D CT reconstruction images were reviewed independently by two observers (B.J. and S.T., with 8-year and 30-year experience in chest radiology, respectively) blinded to the pathologic diagnoses. The final findings for the analyses were determined by consensus of the two observers for categorical data, and averaged values were used for continuous data.

Nodule size (the maximum dimensions on transverse CT images), vertical diameter (the greatest craniocaudal dimensions of a nodule on coronal or sagittal images), the length (the greatest contact length on transverse, coronal, or sagittal CT images) and the area (Fig 1) of the interface between the tumor and the pleura, and the ratios of length (R_{length}) and the area (R_{area}) of the interface between tumor and the pleura to tumor size were assessed. We manually drew the interface between the tumor and the pleura and measured the distance (Figs 1a,b). The ratio of this distance to tumor size was defined as R_{length}. Next, we calculated the volume of all the voxels that comprise the interface, and the volume was divided by a voxel size of y-axis of CT images (Fig 1c). This value was defined as the area of the interface, and the ratio of the area to tumor size was defined as R_{area} in our study. Although both ends of the interface were determined on a CT image of lung window setting, when a part of the interface was difficult to identify, we used different window settings such as mediastinal window setting. In addition, the angle (acute or obtuse) between the tumor and the adjacent pleura (if either of the both sides showed an obtuse angle, this nodule was regarded as having an obtuse angle), and presence or absence of pleural thickening was assessed. The presence or absence of pleural thickening was evaluated on CT images with mediastinum window setting (level, 40 HU; width, 350 HU), and the other analyses on 2D CT images were made on the CT images with lung window setting (level, −600 HU; width, 1200 HU).

A software package (AZE VirtualPlace, Tokyo, Japan) was used for 3D reconstruction in each case. The 3D reconstruction was done with a volume-rendering algorithm. Initially, the effect of threshold level on the appearance of 3D images was evaluated qualitatively in each case. The optimal threshold values (between −470 HU and −540 HU) were chosen on axial images to best visualize the adjacent pleura and the tumor, and only the pixels of higher than the threshold values were visualized on 3D rendering images. All pixels of the other CT attenuation values were automatically removed, leaving only the tumor, pulmonary vessels, pleura, and the chest wall. If necessary, adjacent bronchi and vessels were manually removed, and the opacity was adjusted for optimal visualization of the 3D rendering images. This process required 3 minutes ± 35 seconds (mean ± SD) per case. Thus, the pleural morphology adjacent to the tumor were assessed and classified in reference to 3D rendering images.

Pleural Patterns on 3D CT

The 3D CT rendering images of the pleura were classified into four patterns (Fig 2) according to the presence or absence of adjacent pleural morphologic changes, presence or absence of indrawn pleura toward tumor, and presence or absence of wrinkling of the indrawn pleura as the following: flat pattern (Fig 2a), flat pleura without any morphologic changes in the adjacent pleura; waving pattern (Fig 2b), wrinkled pleura without pleural indrawn thickening toward tumor; rectangular solid pattern (Fig 2c), indrawn pleural thickening toward tumor, and its shape resembles rectangular solid but not associated with pleural wrinkling of the indrawn pleura. Therefore, the indrawn pleura has broad and narrow sides; skirt-like pattern (Fig 2d), indrawn pleural thickening toward tumor associated with pleural wrinkling of the indrawn pleura. Indrawn pleura looks similar on lateral views of different angles.

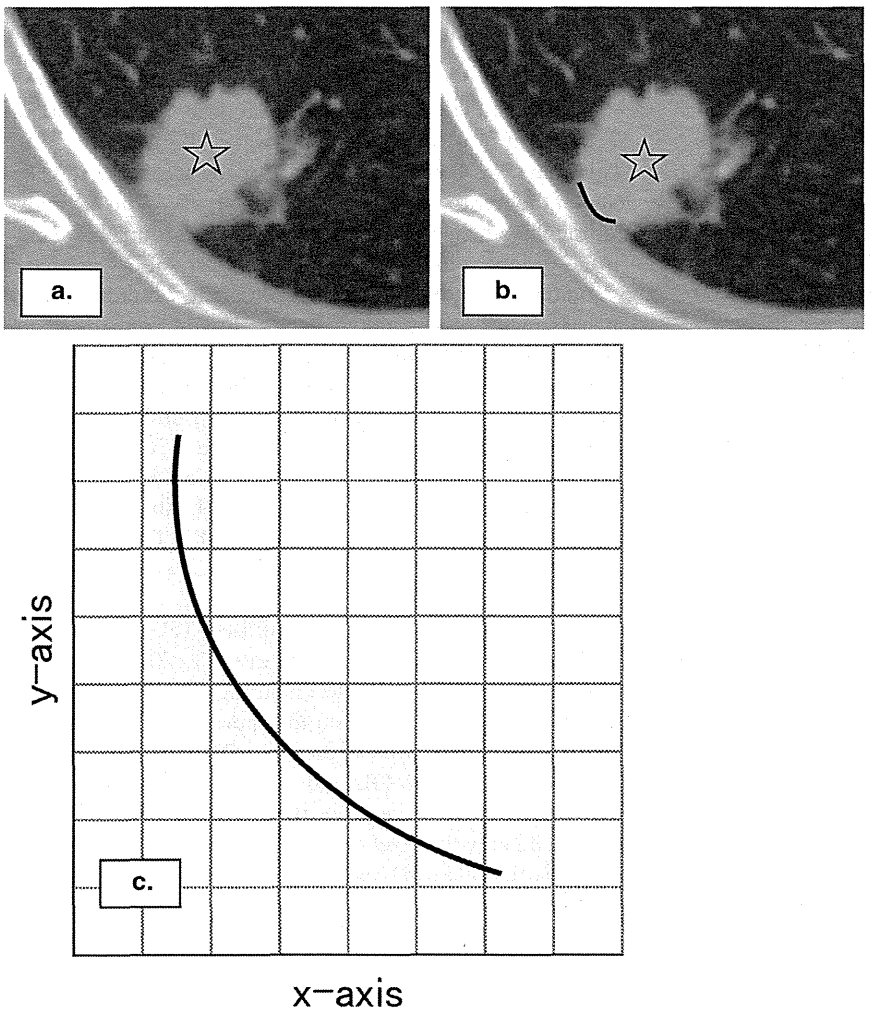

Figure 1. Method of calculation of the area of interface between tumor and the pleura. Transverse computed tomography (CT) image shows a lobulated pulmonary nodule in contact with the chest wall **(a)**. First, we manually drew the interface (*black line*) between tumor and the pleura in all transverse CT sections **(b)** and next calculated the volume of all the voxels (*yellow squares*) that comprise the volume of the interface between tumor and the pleura as shown in an illustration **(c)** and then the volume was divided by a voxel size of y-axis of CT images. This value was defined as the area of the interface in our study. (Color version of figure is available online.)

Pathology

The pathologic specimens stained with hematoxylin–eosin and elastic van Gieson (when necessary) were examined independently to determine the presence or absence and the extent of pleural tumor invasion by two pathologists (Y.T. and M.H. with 20-year and 30-year experience in surgical pathology, respectively), and the final decision on diagnosis was determined by consensus of the two pathologists. Pleural invasion was defined as the following: PL 0, no pleural involvement; PL 1, tumor invasion of the elastic layer of the visceral pleura but without reaching the visceral pleural surface; PL 2, tumor invasion to the visceral pleural surface; PL 3, tumor invasion of the parietal pleura or chest wall (3).

Statistical Analysis

Kappa statistics (for categorical data) and Bland–Altman plots (for continuous data) were carried out to know the inter-observer agreement. The chi-square test or the Fisher exact test for categorical data and the Mann-Whitney *U* test for continuous data were used to examine the significant differences between patients with and without pleural invasion and between patients with visceral and those with parietal pleural invasion. Then, statistically significant factors were assessed with stepwise logistic modeling to determine the most significant factor for predicting pleural invasion. Receiver operating characteristic (ROC) curves were performed to determine the diagnostic capability of the significant factors for predicting the depth of pleural invasion. Finally, we proposed the optimal criteria for predicting pleural invasion and for differentiating parietal from visceral pleural invasion by lung cancer. A P value of $<.05$ was considered to be significant. All the statistical calculations were performed with SPSS software (PASW Statistics 18; SPSS Inc., Chicago, IL).

RESULTS

The size of lung cancers ranged from 0.5 to 2.7 cm, and the histology of lung cancer consisted of 161 adenocarcinomas, 35 squamous cell carcinomas, three large cell carcinomas,

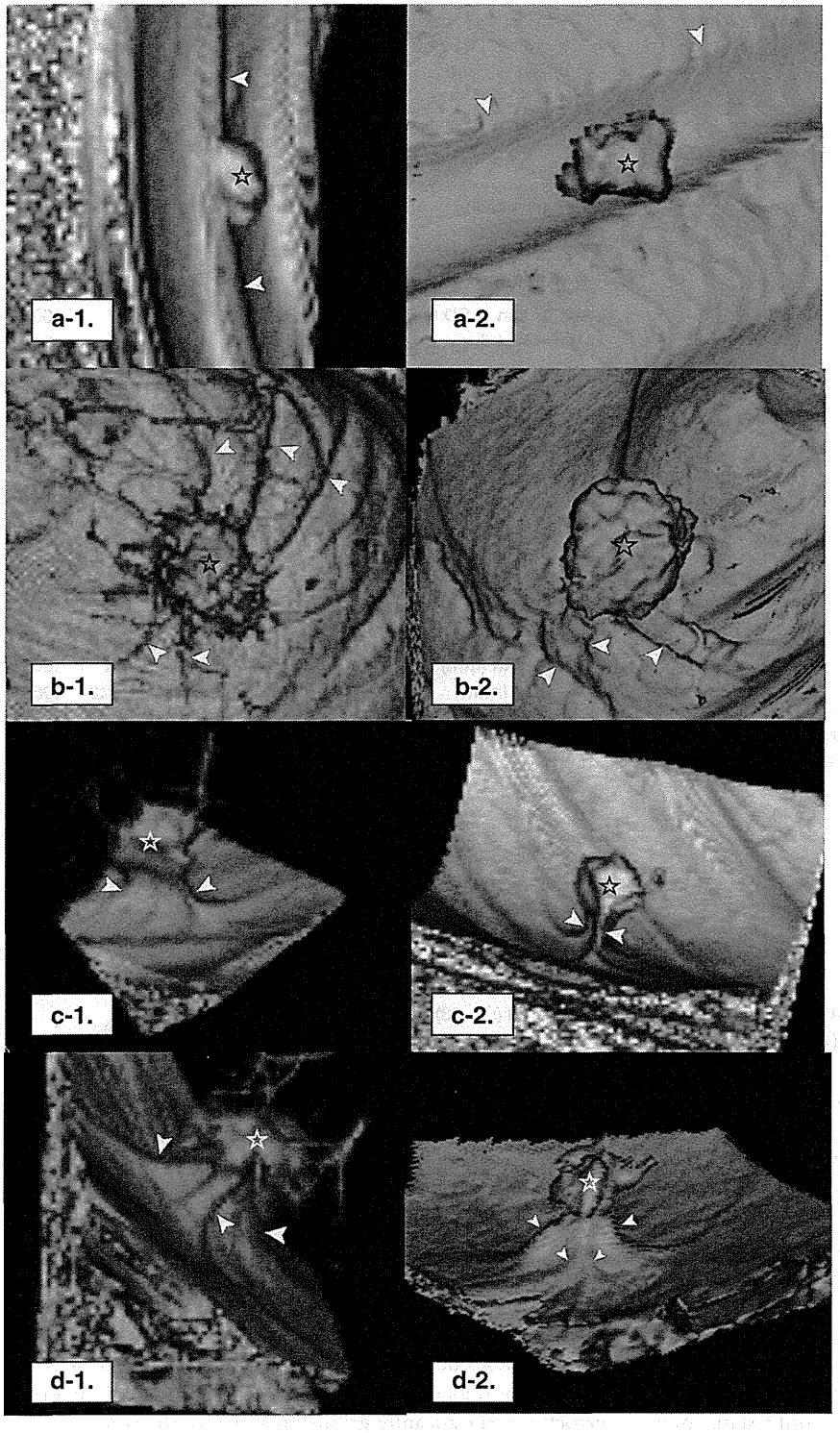

Figure 2. Four 3D CT volume rendering patterns of the pleura. **(a)** Flat pattern: flat pleura without any morphologic changes in the adjacent pleura is seen on both lateral **(a-1)** and top views **(a-2)**. **(b)** Waving pattern: wrinkled pleura without pleural indrawn thickening toward tumor is seen on both top **(b-1)** and acute angle views **(b-2)**. **(c)** Rectangular solid pattern: indrawn pleural thickening without associated pleural wrinkling of the indrawn pleura. Its shape looks rectangular solid. **(c-1)** represents a lateral view of the broad side of the indrawn pleura and another view at right angle of **c-1** shows a narrow side **(c-2)**. No wrinkles are seen in the indrawn pleura. **(d)** Skirt-like pattern: indrawn pleural thickening associated with wrinkling of the indrawn pleura is seen on a lateral view **(d-1)** and it looks similar on another lateral view **(d-2)** at right angle to **d-1**. *Arrowheads* indicate neighboring pleura and *stars* show pulmonary nodules. (Color version of figure is available online.)

and two small cell carcinomas. The neoplasms were pathologically diagnosed as having PL 0 in 140 patients, PL 1 in 38, PL 2 in 14, and PL 3 in nine patients (Table 1). The kappa value was 0.816 for classifying 3D pleural patterns, 0.890 for the angle between tumor and the pleura, and 0.868 for the presence or absence of pleural thickening. The 95% confidence intervals (CIs) for the limits of agreement were −1.7 and 1.8 for tumor size, −1.5 and 1.5 for vertical diameters, −1.8 and 1.9 for the length of interface, −23.1 and 19.6 for the area of interface, −0.13 and 0.14 for the R_{length}, and

TABLE 1. Clinicopathologic Features of 201 Patients with Lung Cancer

Clinicopathologic Features	Data
Patient number	201
Gender (men/women)	126/75
Age, mean ± SD (years)	66.7 ± 9.3
Tumor size, mean ± SD (range) (cm)	1.9 ± 0.6 (0.5–2.7)
Tumor histology	
Adenocarcinoma	161
Squamous cell carcinoma	35
Others	5
Tumor (T stage)	
T1	140
T2	52
T3	9
Node (N stage)	
N0	156
N1	17
N2	28
Grade of pleural invasion	
PL 0	140
PL 1	38
PL 2	14
PL 3	9

PL 0, lack of pleural invasion beyond the elastic layer; PL 1, pleural invasion beyond the elastic layer; PL 2, pleural invasion to the pleural surface; PL 3, pleural invasion into any component of the parietal pleura; SD, standard deviation.

−1.6 and 1.5 for the R_{area}. All these values indicated a good interobserver agreement (7,8).

Pleural Invasion

A significant difference between lung cancer without pleural invasion (PL 0) and with pleural invasion (PL 1–3) was found in gender, tumor size, length of interface, and in 3D pleural patterns (Table 2). Pleural invasion was more frequently seen in men than in women ($P = .017$). Tumor size ($P = .001$) and the length of interface between the tumors and the pleura ($P = .003$) were greater in patients with pleural invasion than patients without invasion ($P = .001$). Although accuracy (34% and 36%, respectively) was poor, sensitivity and negative predictive value for a tumor size of ≥8.2 mm and interface length of ≥4.1 mm were high (100%). Incidence of each 3D pleural pattern was significantly different between the two groups ($P < .001$). Logistic modeling with use of these significant factors as independent variables showed that 3D pleural pattern was the only statistically significant factor ($P < .001$; relative risk of 7.34 with 95% CIs of 3.6 and 14.8). Of every combination of the four 3D pleural patterns, the presence of skirt-like pattern had the highest accuracy of 77% with 59% sensitivity and 85% specificity for predicting pleural invasion (Table 3, Fig 3). There were 21 false-positive and 25 false-negative cases for this optimal criterion.

TABLE 2. Comparison of Clinicopathologic Features and CT Findings in 201 Patients with Lung Cancer with and without Pleural Invasion

Clinicopathologic Features	Pleural Absence (PL 0)	Invasion Presence (PL 1–3)	*P* Value
Patient number	140	61	
Gender, *n* (%)			.017
Men (*n* = 126)	80 (57)	46 (75)	
Women (*n* = 75)	60 (43)	15 (25)	
Age, mean ± SD (years)	65.9 ± 9.5	68.5 ± 8.7	.061
Tumor histology, *n* (%)			.842
Adenocarcinoma (*n* = 161)	111 (79)	50 (82)	
Squamous cell carcinoma (*n* = 35)	25 (18)	10 (16)	
Others (*n* = 5)	4 (3)	1 (2)	
CT imaging findings			
Tumor size, mean ± SD (mm)	14.3 ± 4.9	16.7 ± 4.2	.001
Vertical diameter, mean ± SD (mm)	9.1 ± 7.9	11.9 ± 10.3	.063
Interface, mean ± SD			
Length (mm)	12.0 ± 7.7	15.4 ± 6.8	.003
Area (mm^2)	149.8 ± 184.3	196.9 ± 161.3	.064
Ratio, mean ± SD			
Length/tumor size	0.8 ± 0.3	0.9 ± 0.3	.064
Area/tumor size	9.5 ± 8.6	11.4 ± 7.7	.144
Angle, *n* (%)			.062
Acute (*n* = 144)	106 (76)	38 (62)	
Obtuse (*n* = 57)	34 (24)	23 (38)	
Pleural thickening (*n* = 86), *n* (%)	62 (44)	24 (39)	.539
3D CT pleural patterns, *n* (%)			<.001
Flat (*n* = 81)	71 (51)	10 (16)	
Waving (*n* = 33)	19 (13)	14 (23)	
Rectangular solid (*n* = 30)	29 (21)	1 (2)	
Skirt like (*n* = 57)	21 (15)	36 (59)	

CT, computed tomography; 3D, three dimensional; PL 0, absence of pleural invasion; PL 1, visceral pleural invasion without reaching visceral pleural surface; PL 2, visceral pleural invasion reaching visceral pleural surface; PL 3, parietal pleural invasion.

In differentiating parietal (PL 3) from visceral pleural invasion (PL 1–2), a significant difference was seen in the area of interface ($P = .049$) and the R_{area} ($P = .005$; Table 4). ROC curve analyses demonstrated that the diagnostic capability of R_{area} (areas under the curve [AUC], 0.844 ± 0.051 [standard error]) was significantly greater than that of the area of interface (AUC, 0.794 ± 0.058) for differentiating parietal from visceral pleural invasion ($P = .03$) (9). When a cut-off value of 13.4 was used for the R_{area}, the highest accuracy of 77% with 89% sensitivity and 75% specificity was obtained for differentiating parietal from visceral pleural invasion (Fig 4). There were 13 false-positive cases and one false-negative case for this optimal criterion. A cut-off value of ≥12.1 for

TABLE 3. Diagnostic Statistics of CT Findings for Predicting Pleural Invasion

Predictors	Sensitivity, %	Specificity, %	Accuracy, %	PPV, %	NPV, %
CT imaging measurements					
Tumor size, mm					
≥8.2	100	5	34	31	100
≥19.4	33	87	71	53	75
Length of interface, mm					
≥4.1	100	9	36	32	100
≥17.6	36	86	71	52	76
3D CT pleural patterns					
Flat pattern	84	51	61	43	88
Rectangular solid pattern	98	21	44	35	97
Waving pattern	23	86	67	42	72
Skirt-like pattern	59	85	77	63	83
Skirt-like or waving pattern	82	71	75	56	90
Skirt-like or flat pattern	75	34	48	33	76
Skirt-like or rectangular solid pattern	61	64	63	43	79

CT, computed tomography; 3D, three dimensional; NPV, negative predictive value; PPV, positive predictive value.

the R_{area} yielded 100% sensitivity, but its accuracy (70%) and specificity (65%) was not high.

DISCUSSION

Diagnosis of the presence or absence and the depth of pleural invasion with CT are clinically important because T staging depends on the P staging, and therefore, an appropriate treatment method and prognosis are greatly influenced by P staging. Regarding the prognosis of patients with T1-sized NSCLC, the 5-year survival rate is reported to worsen as the P staging advances as follows (3): 86% for patients with PL 0 (T1), 62% for patients with PL 1 (T2), 70% for patients with PL 2 (T2), and 57% for patients with PL 3 (T3). As for the surgical method, T1 or T2 tumors are resectable with standard surgical techniques, whereas en bloc resection of the chest wall invaded by tumor is recommended for T3 tumors (10,11). Therefore, the separation of T3 tumors with imaging techniques before surgery is clinically more important than the separation of T2 and T1 stage tumors. Adjuvant chemotherapy may be required for patients after complete resection of tumors with pleural invasion (12).

On 2D CT findings, our study showed that tumor size and length of interface between tumor and the pleura were significantly greater in tumors with pleural invasion than those without pleural invasion. Although these two findings proved to be of no statistical significance for diagnosing pleural invasion based on the multivariate analysis, both findings showed 100% sensitivity and 100% negative predictive value. Therefore, we think patients who have a tumor size of <8.2 mm or who have an interface length of <4.1 mm determined with preoperative CT may be reliably diagnosed as having no pleural invasion by tumor (clinical T1 tumor).

There are several reports on diagnosing pleural invasion by lung cancer with the use of 2D CT imaging findings (4,5). Glazer et al. (4) stated that the angle and the length of interface between the tumors and the pleura, and associated pleural thickening were of value in predicting pleural invasion, and the authors mentioned that the combination of two or three of these CT findings resulted in 68% accuracy with 87% sensitivity and 59% specificity. In our study, although the interface length was a significant predictor for pleural invasion as documented by Glazer et al., the other factors were of no significance for diagnosing pleural invasion. These discordant results may be caused by the difference in patients' population and CT parameters. Compared to our study, Glazer et al. used thicker CT collimation (8 or 1 cm) and included larger tumors (more than half of the patients had lung cancer of ≥3 cm) and smaller number of patients ($n = 47$). Furthermore, we think that all the three predictors proposed by Glazer et al. can be more accurately appreciated with thin-section CT as used in our study than with thick-section CT as used in the series of Glazer et al.

Recently, Imai et al. (13) studied 2D CT imaging findings scanned with 1.25–5 mm CT collimations in 169 lung cancers of ≥3 cm to determine the useful factors for predicting pleural invasion and reported that the ratio of interface length between the tumor and the pleura to the maximum tumor diameter (corresponding to R_{length} in our study) achieved high accuracy exceeding 90% for predicting T3 or T4 tumors. However, our data showed the R_{length} was not useful for predicting pleural invasion or in differentiating T3 from T2 invasion. This contradictory result may be largely caused by the difference in tumor size. In the present series, we dealt with

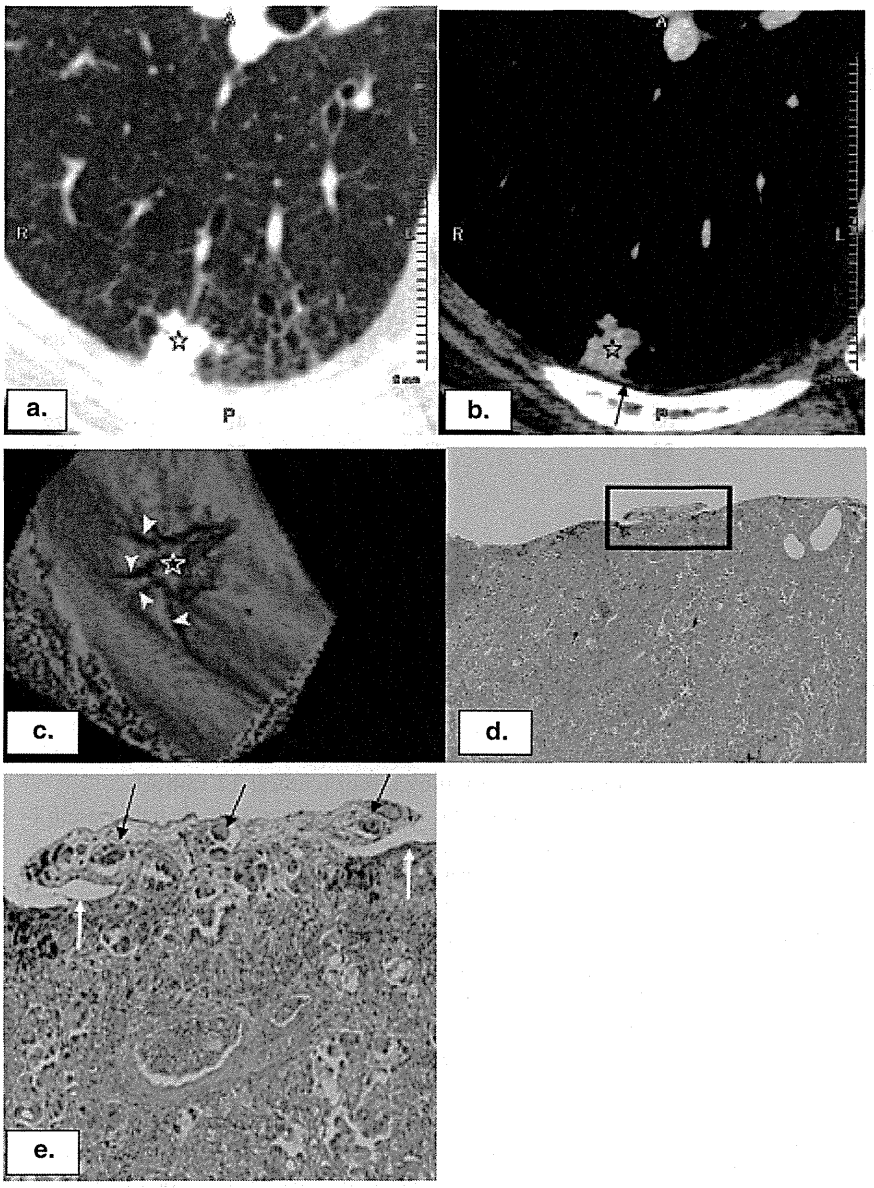

Figure 3. Adenocarcinoma with visceral pleural invasion in a 64-year-old man. A 14-mm pulmonary nodule (*star*) in contact with the pleura over 9.5 mm **(a)** and associated faint pleural thickening (*arrow* in **b**) are seen. 3D rendering CT imaging demonstrated a skirt-like pattern (arrowheads) of the pleura that suggested pleural invasion by lung cancer **(c)** The R_{area} calculated on 3D CT images with computer aid was 10.3, which was below the optimal threshold of R_{area} of 13.4 for predicting parietal pleural invasion. Therefore, the R_{area} correctly predicted visceral pleural invasion by lung cancer. Low-power micrograph **(d)**: hematoxylin–eosin stain; original magnification, ×40) of the resected specimen showed a tumor in contact with the pleura. High-power micrograph **(e)**: hematoxylin–eosin stain; original magnification, ×200) of the rectangular area in **c** revealed tumor invasion of the visceral pleura with tumor cells (*black arrows*) spreading on the surface of the visceral pleura (*white arrows*). Pleural invasion was correctly diagnosed with 3D CT images. (Color version of figure is available online.)

the T1-sized tumors only because the stage-shift effect of P staging in T factor is greater in T1-sized tumors than in larger tumors. As Imai et al. (13) dealt with only tumors of >3 cm, the researchers did not address the issue of separation of T1 and T2 tumors. Although separation of T1 and T2 tumors does not impact management, this will afford different prognostic information. Therefore, this separation will be also clinically important. We think that the criteria proposed by Imai et al. may be useful for prediction of T3 and T4 tumors, whereas our criteria may be useful for separation of T1 and T2 tumors of <3 cm.

Kuriyama et al. (6) reported that 3D CT imaging was superior to the conventional criteria on 2D CT imaging proposed by Glazer et al. (4) in the assessment of pleural invasion in a series of 42 patients with lung cancer. The authors stated that pleural puckering as defined as localized thickening of the pleura that was indrawn toward the tumor on 3D CT imaging showed the highest accuracy of 79% with 82% sensitivity and 76% specificity for prediction of pleural invasion by lung cancer. However, Kuriyama et al. evaluated only the conventional criteria on 2D CT imaging and addressed only the utility of pleural puckering on 3D CT imaging. In the present study, we evaluated almost all the quantitative and qualitative findings on 2D CT imaging and possible other pleural patterns such as flat, waving, rectangular solid, or skirt-like pattern and 3D measurements, including R_{area} on 3D CT imaging. Furthermore, the number of patients in the series of Kuriyama et al. was far smaller

TABLE 4. Comparison of Clinicopathologic Features and CT Findings Between 52 Patients with Visceral Pleural Invasion and Nine Patients with Parietal Pleural Invasion

Features	Visceral Pleural Invasion (PL 1–2)	Parietal Pleural Invasion (PL 3)	*P* Value
Patient number	52	9	
Gender, *n* (%)			.676
Men (*n* = 46)	40 (77)	6 (67)	
Women (*n* = 15)	12 (23)	3 (33)	
Age, mean ± SD (years)	68.3 ± 8.6	70.2 ± 9.7	.536
Tumor histology, *n* (%)			.313
Adenocarcinoma (*n* = 50)	41 (79)	9 (100)	
Squamous cell carcinoma (*n* = 10)	10 (19)	0 (0)	
Other (*n* = 1)	1 (2)	0 (0)	
Findings on CT images			
Tumor size, mean ± SD (mm)	16.8 ± 4.3	16.3 ± 3.3	.755
Vertical diameter, mean ± SD (mm)	10.8 ± 8.7	11.8 ± 9.9	.521
Interface, mean ± SD			
Length (mm)	15.1 ± 7.0	17.3 ± 5.4	.365
Area (mm^2)	180.1 ± 163.0	294.2 ± 115.5	.049
Ratio, mean ± SD			
Length/tumor size	0.9 ± 0.3	1.1 ± 0.3	.139
Area/tumor size	10.3 ± 7.6	17.9 ± 4.8	.005
Angle, *n* (%)			.278
Acute (*n* = 38)	34 (65)	4 (44)	
Obtuse (*n* = 23)	18 (35)	5 (56)	
Pleural thickening (*n* = 24), *n* (%)	20 (38)	4 (44)	.729
3D CT pleural patterns, *n* (%)			.474
Flat (*n* = 10)	10 (19)	0 (0)	
Waving (*n* = 14)	11 (21)	3 (33)	
Rectangular solid (*n* = 1)	1 (2)	0 (0)	
Skirt like (*n* = 36)	30 (58)	6 (67)	

CT, computed tomography; 3D, three dimensional; PL 1, visceral pleural invasion without reaching visceral pleural surface; PL 2, visceral pleural invasion reaching visceral pleural surface; PL 3, parietal pleural invasion; SD, standard deviation.

than ours. Nonetheless, the accuracy (79%) of pleural puckering reported by Kuriyama et al. was comparable to that (77%) of the optimal criterion of skirt-like pattern proposed in our study. Thus, we suggest the possibility of pleural invasion is high for the patients who have a skirt-like pleural pattern on preoperative 3D CT and therefore, a prompt treatment should be required, and the possibility of use of more aggressive surgery than standard technique in addition to probable poorer prognosis should be informed to these patients before surgery.

Pathologically, tumor invasion of the thick elastic fiber layer of visceral pleura is regarded as a hallmark of pleural invasion, and this fiber is responsible for pleural mechanical stability (2). The geometric and mechanical properties of the elastic fiber are affected by tumor invasion, and the resultant effect is graded into three patterns: without eliciting any secondary changes, with prominent elastic reduplication and inflammatory infiltrate, and with thick fibroblastic proliferation (14). The pleural wrinkling is considered to be caused by the disruption of pleural mechanical stability such as by direct tumor invasion and by secondary changes of tumor invasion (15). Therefore, pleural wrinkling with indrawn thickening may represent pleural invasion by lung cancer (6). In our study, this sign was associated mainly with skirt-like pleural pattern on 3D CT imaging. However, minimal invasion of the visceral pleura may not result in a significant pleural change, and on the contrary, inflammatory process without tumor invasion may cause a significant pleural change. These pathologic changes may have caused false-positive and false-negative cases for our optimal criterion of skirt-like pleural pattern in our study.

Our study demonstrated that the R_{area} was beneficial for differentiating parietal from visceral pleural invasion by lung cancer, which has not been documented in the previous literature. Our series demonstrated the R_{area} of >13.4 had the highest accuracy of 77% with 89% sensitivity and 75% specificity for differentiating parietal from visceral pleural invasion. As the R_{area} becomes greater, the contact area between the tumor and the pleura will be more extensive, presumably resulting in deeper tumor invasion to the pleura such as to the parietal pleura. Because the R_{area} eliminates the effect of tumor size, it may be applied to lung cancer irrelevant to their tumor size. Although the R_{area} is applicable only to the patients after surgical resection of the tumor with subsequent pathologic proof of pleural invasion, when the patient have the R_{area} of >13.4 on preoperative 3D CT, the information

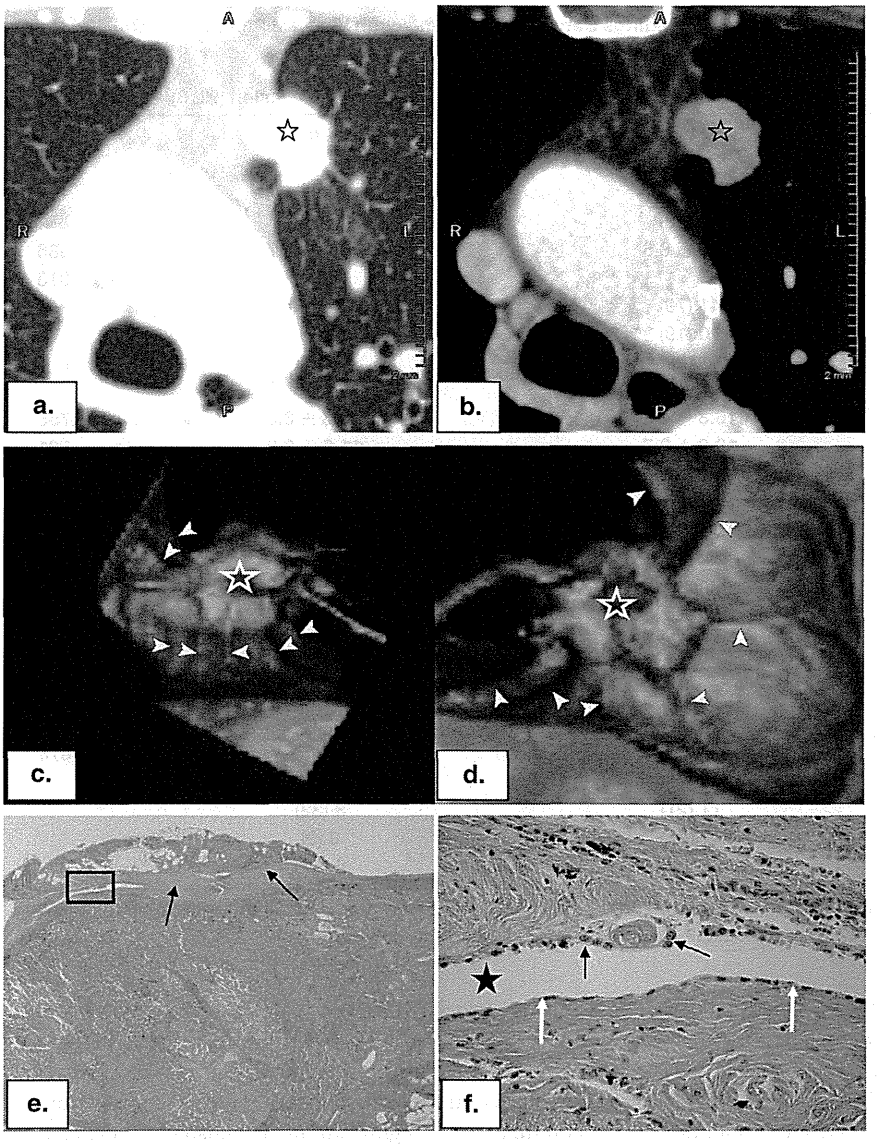

Figure 4. Adenocarcinoma with parietal pleural invasion in a 58-year-old woman. A 17-mm pulmonary nodule (*star*) in contact with the pleura >13.7 mm **(a)** and no associated pleural thickening **(b)** are seen. 3D rendering CT imaging demonstrated a skirt-like pattern of the pleura [**(c** and **d)**; **(c)** lateral view; **(d)** view as seen from above.] Calculated R_{area} was 17.6, which exceeded the optimal threshold of R_{area} of 13.4 for diagnosing parietal pleural invasion, and therefore, parietal pleural invasion was correctly predicted with our criterion. Low-power micrograph **(e)** hematoxylin–eosin stain; original magnification, ×40) of the resected specimen showed local pleural adhesion (*arrows*) in the neighboring area of the tumor. High-power micrograph [**(f)** hematoxylin–eosin stain; original magnification, ×200] of the rectangular area in **e** revealed subtle tumor invasion in the parietal pleura (*black arrows*). *Star*, pleural cavity; *white arrow*, surface of visceral pleura. (Color version of figure is available online.)

of the possibility of en bloc resection of the chest wall can be provided to the patients and surgeons before surgery.

There are several limitations in our study. First, the number of patients with parietal pleural invasion was too small to draw a conclusion regarding the usefulness of R_{area} in differentiating parietal from visceral pleural invasion. Second, our criteria for predicting pleural invasion are applicable only to T1-sized lung cancer. Third, the R_{area} is applicable only to the patients who had pathologically verified pleural invasion by lung cancer and therefore, cannot be a preoperative predictor. Finally, it took relatively long time to make the 3D rendering images and calculate the R_{area}. More simple and sophisticated method should be developed.

In summary, the 3D data can give information regarding pleural involvement and prognosis, and it can help the surgeon plan a most adequate approach to resect the T1-sized lung cancer.

ACKNOWLEDGMENTS

The authors thank Gen-ichiro Yoneda, MD (Department of Pathology), for analyzing pathologic data.

REFERENCES

1. UyBico SJ, Wu CC, Suh RD, et al. Lung cancer staging essentials: the new TNM staging system and potential imaging pitfalls. Radiographics 2010; 30(5):1163–1181.
2. Travis WD, Brambilla E, Rami-Porta R, et al. Visceral pleural invasion: pathologic criteria and use of elastic stains: proposal for the 7th edition of the TNM classification for lung cancer. J Thorac Oncol 2008; 3(12): 1384–1390.
3. Oyama M, Miyagi Maeshima A, Tochigi N, et al. Prognostic impact of pleural invasion in 1488 patients with surgically resected non-small cell lung carcinoma. Jpn J Clin Oncol 2013; 43(5):540–546.
4. Glazer HS, Duncan-Meyer J, Aronberg DJ, et al. Pleural and chest wall invasion in bronchogenic carcinoma: CT evaluation. Radiology 1985; 157(1):191–194.

5. Pennes DR, Glazer GM, Wimbish KJ, et al. Chest wall invasion by lung cancer: limitations of CT evaluation. AJR 1985; 144(3):507–511.
6. Kuriyama K, Tateishi R, Kumatani T, et al. Pleural invasion by peripheral bronchogenic carcinoma: assessment with three-dimensional helical CT. Radiology 1994; 191(2):365–369.
7. Blum A, Feldmann L, Bresler F, et al. Value of calculation of the kappa coefficient in the evaluation of an imaging method. J Radiol 1995; 76(7):441–443.
8. Bland JM, Altman DG. Comparing methods of measurement: why plotting difference against standard method is misleading. Lancet 1995; 346(8982):1085–1087.
9. Hanley JA, McNeil BJ. A method of comparing the areas under receiver operating characteristic curves derived from the same cases. Radiology 1983; 148(3):839–843.
10. DiPerna CA, Wood DE. Surgical management of T3 and T4 lung cancer. Clin Cancer Res 2005; 11(13 Pt 2):5038s–5044s.
11. Facciolo F, Cardillo G, Lopergolo M, et al. Chest wall invasion in non-small cell lung carcinoma: a rationale for en bloc resection. J Thorac Cardiovasc Surg 2001; 121(4):649–656.
12. Tsuboi M, Ohira T, Saji H, et al. The present status of postoperative adjuvant chemotherapy for completely resected non-small cell lung cancer. Ann Thorac Cardiovasc Surg 2007; 13(2):73–77.
13. Imai K, Minamiya Y, Ishiyama K, et al. Use of CT to evaluate pleural invasion in non-small cell lung cancer: measurement of the ratio of the interface between tumor and neighboring structures to maximum tumor diameter. Radiology 2013; 267(2):619–626.
14. Gallagher B, Urbanski SJ. The significance of pleural elastica invasion by lung carcinomas. Hum Pathol 1990; 21(5):512–517.
15. Shimosato Y, Suzuki A, Hashimoto T, et al. Prognostic implications of fibrotic focus (scar) in small peripheral lung cancers. Am J Surg Pathol 1980; 4(4):365–373.

（肺癌．2014;54:121-127）

ORIGINAL ARTICLE

肺癌術後経過観察中に発見された孤立性充実性肺悪性病巣に対する外科治療成績の検討

藤原綾子[1]・東山聖彦[1]・狩野　孝[1]・徳永俊照[1]・
岡見次郎[1]・井上敦夫[2]・冨田裕彦[3]・今村文生[4]

Surgical Outcomes of Solitary Solid Malignant Lung Nodules Detected During Follow-up After Resection of Primary Lung Cancer

Ayako Fujiwara[1]; Masahiko Higashiyama[1]; Takashi Kanou[1]; Toshiteru Tokunaga[1]; Jiro Okami[1]; Atsuo Inoue[2]; Yasuhiko Tomita[3]; Fumio Imamura[4]

[1]Department of General Thoracic Surgery, [2]Department of Radiology, [3]Department of Pathology and Cytology, [4]Department of Respiratory Medicine, Osaka Medical Center for Cancer and Cardiovascular Diseases, Japan.

ABSTRACT —— ***Objective.*** To review the diagnostic accuracy and surgical outcomes of solitary solid malignant lung nodules diagnosed as either second primary lung cancer (SPLC) or lung metastasis (LM) detected during follow-up after resection of primary lung cancer. ***Methods.*** The subjects included 54 primary lung cancer patients who underwent more than one lung resection procedure and were diagnosed with SPLC or LM between January 1976 and December 2010. We performed a retrospective comparative review of these two groups. ***Results.*** There were 35 SPLC patients and 19 LM patients. The background factors, including age and smoking history, were similar between the two groups. In 17 patients (31.5%), there were differences between the preoperative clinical diagnosis and postoperative pathological diagnosis. The median survival time for all patients after the second surgery was 61.9 months. The median survival time was 61.6 months in the LM patients and 60.9 months in the SPLC patients, which was not significantly different (P = 0.77). The recurrence rate after the second operation was significantly higher in the LM patients (P = 0.007). The most common site of recurrence in the LM patients was the pleural space, with repeat lung metastases being especially common. ***Conclusions.*** In the present study, the surgical outcomes of solitary solid malignant lung nodules detected during follow-up after primary lung cancer resection were relatively favorable, with a five-year survival rate of 60.8%. Therefore, such patients are considered to be indicated for surgery. The pattern of recurrence after the second surgeries differed between the SPLC and LM patients; therefore, close follow-up is required.

(*JJLC.* 2014;54:121-127)

KEY WORDS —— Primary lung cancer, Solitary solid lung nodule, Second primary lung cancers, Lung metastasis, Surgical resection

Reprints: Masahiko Higashiyama, Department of General Thoracic Surgery, Osaka Medical Center for Cancer and Cardiovascular Diseases, 1-3-3 Nakamichi, Higashinari-ku, Osaka-shi, Osaka 537-8511, Japan.

Received December 12, 2013; accepted March 27, 2014.

要旨 —— **目的．** 肺癌術後経過観察中の患者に出現した孤立性充実性病巣のうち，悪性疾患（2次性原発性肺癌（SPLC）または肺癌再発（LM））に対する診断精度や手術成績を検討した．**方法．** 1976年1月から2010年12月までの間に当院で切除を行った原発性肺癌症例中，複数回の肺切除が行われSPLCまたはLMと診断された54例を対象とし，後ろ向きに比較検討した．**結果．** 2回目手術の病理学的診断は，SPLC 35例，LM 19例．背景因子に2群間で有意差を認めなかった．全症例の2回目術後生存期間中央値は61.9ヶ月，群別ではLMが61.6

大阪府立成人病センター [1]呼吸器外科，[2]放射線診断科，[3]病理・細胞診断科，[4]呼吸器内科．
別刷請求先：東山聖彦，大阪府立成人病センター呼吸器外科，〒537-8511　大阪府大阪市東成区中道1-3-3.
受付日：2013年12月12日，採択日：2014年3月27日．

ヶ月，SPLCが60.9ヶ月で，有意差を認めなかった(P＝0.77)．2回目手術以降の経過について検討したところ，LM群で有意に再発頻度が高く(P＝0.007)，再発様式は，LM群では胸腔内，特に肺内転移の再々発が有意に多かった．**結論．**肺癌切除後に発見された孤立性充実性肺悪性病変に対する外科切除後の成績は5年生存率60.8%と比較的良好で，積極的に手術適応と考えられる．その後の再発様式は，SPLCとLMでは異なり，経過観察に配慮が必要である．

索引用語 —— 原発性肺癌，孤立性充実性肺結節，2次性原発性肺癌，肺癌再発，外科治療

はじめに

肺癌術後経過観察中に新たに孤立性肺病巣を発見した場合，悪性疾患に限れば，1) 前回肺癌の再発，2)2次性原発性肺癌，3)他悪性疾患の肺転移が考えられる．肺癌術後患者で再発が最も多いのは胸腔内で，全再発の約56% を占める報告がある一方，[1] 新たに肺癌あるいは他臓器癌を発症(異時性多発癌，多重癌)する頻度も高く，特に喫煙者では約10倍も高率であることが示されている．またJohnsonらは，非小細胞癌切除後患者では2次性原発性肺癌発症のリスクは年に1〜2% と報告している．[2]

ところでこのような孤立性肺病巣において，1)前回肺癌の再発 (lung metastasis，LM) か，2)2次性原発性肺癌(second primary lung cancer，SPLC)かの鑑別診断には，1975年に報告されたMartiniらの臨床病理学的基準が現在でも広く用いられている．[3] 彼らの鑑別診断基準によれば組織型が最も重要な項目に挙げられているが，その術前に行う気管支鏡検査では，初回肺切除後であること，十分量の検体が得られないことなどから，結局，鑑別診断が困難なことも多い．

一方，近年，高分解能CTが導入され，肺病巣を詳細に観察できるようになり診断能は著しく向上した．その結果，肺癌の陰影で主にすりガラス陰影 (GGO) を呈する場合には原発性と診断され，[4,5] たとえ複数の陰影や肺癌既往があっても多発肺癌と診断されるようになった．しかし，充実性結節陰影を呈する肺病巣に関しては，たとえ高分解能CTでもLMかSPLCかの鑑別はしばしば困難で，臨床ではその診断と治療方針決定に難渋することが多い．

今回，我々は当院で原発性肺癌術後経過観察中に出現した孤立性充実性肺病巣に対し，外科切除を行い病理学的にLMまたはSPLCと診断された症例を対象に，これら症例の2回目手術の術前診断，手術治療および転帰を見直し，その診断精度や治療成績を後ろ向きに検討した．

対象および方法

1976年1月から2010年12月までの間に当院で切除を行った原発性肺癌4125例中，複数回の肺切除が行われた症例は314例であった．このうち2回目手術前のCT画像が孤立性充実性結節陰影を示した症例で，切除標本の病理学的検討にてLMまたはSPLCと確定診断がなされた54例が対象である．術前高分解能CTにてGGOを呈した症例や，術後断端再発と診断された症例は除外した．

なお充実性結節陰影とは，高分解能CTにてほぼ全てが軟部組織吸収値を呈する陰影とし，内部に肺血管や気管支を透亮できGGOと定義されている陰影を少しでも含む症例[6]は，今回の対象外とした．

また，2回目手術の適応として，前述の肺結節の条件以外に，1)肺以外に転移性を疑わせる病変がないこと，2)呼吸機能を含め耐術能を満たしていること，3)他に悪性病変がないこと，を原則とした．

これら54病変に対する2回目手術の術前診断は，CTや気管支鏡検査の所見に加え，臨床的背景を考慮し呼吸器外科医，呼吸器内科医，放射線科医合同カンファレンスで得られた診断を術前診断とした．確定診断は，2回目手術時標本と初回手術標本とを2名以上の病理専門医が比較検討して行った．病理組織学的に，2回目標本の組織型が前回と同一であった症例では，細胞形態や分化度の異同，脈管侵襲，周囲組織への浸潤パターンなどに注目し，2回目標本組織で，脈管侵襲や壊死が著しい症例ではLMを，気管支粘膜内進展や肺胞上皮進展が少しでも観察される症例はSPLCを念頭に置き，慎重に診断した．

具体症例を示す (Figure 1)．症例1 (Figure 1a) は，肺腺癌 (p-stage IA) にて右下葉切除，初回手術後1年3ヶ月して左上葉に13 mm大の孤立性充実性結節を指摘され，術前診断はLM，左上葉部分切除を施行した．2回目標本では，肺腺癌で，前回の切除標本と類似しており，多数の脈管侵襲を認めたため，LMと診断した．症例2 (Figure 1b) は，肺高分化型扁平上皮癌にて左肺摘除 (p-stage IB) した症例で，術後6年目に右肺下葉に18 mm大の孤立性充実性結節を指摘された．気管支鏡検査では扁平上皮癌と診断されたが，検体量が少なくLMかSPLCかの鑑別は困難であった．右肺下葉部分切除術を行い，低分化型扁平上皮癌のためSPLCと診断した．

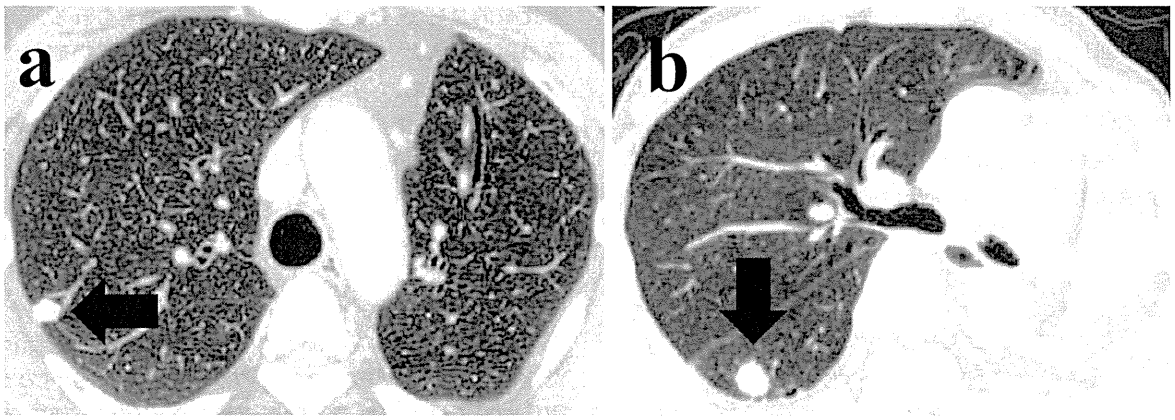

Figure 1. CT scans in representative cases. **a.** A 13-mm solid nodule was detected in the left upper lobe one year and three months after lung cancer surgery. The tumor was diagnosed as lung metastasis based on a pathological examination. **b.** An 18-mm solid nodule was detected in the right lower lobe six years after lung cancer surgery. The tumor was diagnosed as a lesion of multiple lung cancer. The lesions in **a** and **b** were both well-circumscribed, round, solid nodules that were difficult to classify as lung metastasis (LM) or second primary lung cancer (SPLC).

術後成績は，2回目手術日を起点としたKaplan-Meier法にて生存率を算出し，有意差検定にはlog-rank testを用いた．$P<0.05$を有意とした．

結　果

患者背景

全症例の初回および2回目手術に関する臨床病理学的所見をTable 1に示す．男性36例，女性18例で，1回目手術時の平均年齢は63（48～78）歳，2回目手術では67（51～79）歳で，手術間隔の中央値は66.9（2.6～137.8）ヶ月であった．初回手術時のp-stageは，各々p-stage IA（18例）/IB（25例）/IIA（1例）/IIB（3例）/IIIA（6例）/IIIB（1例）であった．初回手術では，54例中44例（81.5%）で葉切除以上が行われていたが，2回目手術では54例中40例（74.1%）が縮小手術であった．組織型は，1回目，2回目手術ともに腺癌が最も多く，次いで扁平上皮癌の順であった．なお2回目手術の術前診断は，気管支鏡的診断症例が3例，辺縁形態や胸膜陥入の有無，増大速度など画像的診断が25例，初回肺癌の進行度や分化度，初回肺癌手術からの期間など臨床背景に基づき診断した症例が26例で，18例（33.3%）をLM，36例（66.7%）をSPLCと診断した．術後診断はLMが19例，SPLCが35例となった．

全症例の，2回目手術からの生存期間中央値は61.9ヶ月，5年生存率は60.8%であった．

2回目手術時組織学的確定診断について

病理専門医の検討に基づき最終的に診断し，LM 19例，SPLC 35例であった．LM 19例に関しては，組織型が同一で，さらに細胞形態が類似していることを基本条件とし，脈管侵襲や壊死などを付加的に考慮して決定した．SPLCでは11例で組織型が異なっていたが，24例では組織型は同一であった．同一組織型の症例で，SPLCと診断した主な理由は，肺胞上皮進展の有無や分化度の差が10例で最も多く，次いで癌細胞の核異型度，細胞自体の大きさや形態の差が6例（例えば，II型肺胞上皮への分化またはクララ細胞への分化などの差），腺構造の差が5例（例えば，乳頭状構造または腺房構造の差），脈管侵襲の程度・有無が2例，免疫染色の差が1例（TTF-1，CK7，CK20，Napsin Aなど）であった．

LM症例とSPLC症例の比較

LM症例とSPLC症例の2群間比較を行った．結果をTable 2に示す．

LM群で年齢が若い傾向があったが，有意差は認めなかった（$P=0.09$）．喫煙歴の有無，1回目手術からの期間，1回目手術時の肺癌のstageについても2群で差を認めなかった．

術前診断と術後診断

2回目術前診断と術後病理組織学的診断が合致していたのは，54例中37例（68.5%）で，LM群で19例中10例（52.6%），SPLC群で35例中27例（77.1%）となった．逆に，17例（31.5%）の症例で術前診断と病理組織学的診断の不一致が見られた．

手術術式

2群で2回目手術術式に差を認めなかった．

病理組織

2回目手術時の腫瘍サイズおよび胸腔内リンパ節転移の有無については，2群間に差を認めなかった．SPLC群で初回肺癌と2回目の肺癌の組織型が一致した割合

Table 1. Background Factors Before the Second Surgery in All 54 Patients

Variables	First surgery	Second surgery
Gender Male/Female	36/18	
Age (median, years)	63 (48-78)	67 (51-79)
Interval from previous surgery (median, months)	-	66.9 (2.6-137.8)
Surgical method		
Pneumonectomy	2	3 (completion)
Lobectomy	42	11
Segmentectomy	8	13
Wedge resection	2	27
Pathological stage at first surgery		
IA/IB/IIA/IIB/IIIA/IIIB/IV	18/25/1/3/6/1/0	-
Tumor size		
≤3 cm	25	41
>3 cm	29	12*
Lymph node metastasis		
Negative	44	13
Positive	8	7
Not done	2	34
Pathology		
Adenocarcinoma	33	27
Squamous cell carcinoma	19	22
Adenosquamous carcinoma	1	2
Large cell carcinoma	1	1
Small cell carcinoma	0	2
Clinical diagnosis at second surgery		
Lung metastasis	-	18
Second primary lung cancer	-	36
Survival after surgery (median, months)	123.4	61.9

*The tumor size was unknown in one patient.

は，35例中24例（68.6%）であった．

2回目手術後転帰

2回目手術以降の再発について検討したところ，LM群で有意に再発頻度が高かった（P＝0.007）．再発様式では，胸腔外遠隔転移の再発に関しては2群間に有意差を認めなかったが，胸腔内再発と特に肺内転移の再々発に関しては，有意にLM群で多かった（胸腔内再発；P＝0.001，肺内転移再々発；P＝0.002）．

両群の生存期間中央値はLM；61.6ヶ月，SPLC；60.9ヶ月，5年生存率はLM；56.0%，SPLC；61.0%で，これら2群間に有意差を認めなかった（P＝0.77）（Figure 2）．

経過観察中に死亡した27例（LM群；11例，SPLC群；16例）の死因を検索したところ，肺癌死はLM群で11例中8例（72.7%），SPLC群で16例中9例（56.3%）であった．

考　察

原発性肺癌術後経過中に新たに出現した孤立性肺病巣では，CT画像でGGOが主立った症例は，通常，新たな原発性肺癌（SPLC）として扱われている．一方GGOを含まない充実性結節陰影は，病理学的に浸潤性あるいは膨張性進展した病巣が多く，LMか，SPLCかの鑑別診断が画像のみでは困難なことが多い．しかし，特に2回目の術前診断は，本来，治療方法の選択にも関わってくることであり，その精度に関しては興味が持たれる．しかしながら，LMやSPLCについての見解は多数報告されているものの多くが2回目切除後の組織学的診断に基づいた検討であり，術前診断の精度について検討を加えた報告はほとんどない．今回の検討は当施設の成績を後ろ向きに行ったものであるが，術前診断について言及したほぼ唯一の報告であり，今後の診断治療に意義あるものと考えている．

今回の検討では，複数の呼吸器科医および放射線診断医が術前に検討した結果，術前診断と術後診断の一致は68.5%程度であった．気管支鏡検査または経皮的肺穿刺を行い術前診断が得られたのは3例のみで，通常，画像所見と臨床情報のみで術前診断を検討せねばならない．診断一致率が低い理由として，病巣が初回肺癌の経過観察中に発見されるため比較的小さく特徴に乏しいことや，肺切除歴があるため気管支鏡による診断困難なこと

Table 2. Clinicopathological Characteristics at the Second Surgery -Lung Metastasis (LM) vs Second Primary Lung Cancer (SPLC)-

Variables	LM (N=19)	SPLC (N=35)	P
Age (median, years)	66 (51-77)	69 (54-79)	0.08
Smoking history			
No	6	11	> .99
Yes	13	24	
Interval from previous surgery (median, months)	47.4 (11.3-112.5)	55.1 (1.4-132.8)	0.83
p-stage of the preceding cancer			
IA/IB	15	28	> .99
IIA/IIB/IIIA/IIIB	4	7	
Clinical diagnosis			
Lung metastasis	10	8	
Second primary lung cancer	9	27	
Surgical method*			
Pneumo or Lobe	4	10	0.74
Seg or Wedge	15	25	
Tumor size†			
≤3 cm	14	27	0.95
>3 cm	4	8	
Lymph node metastasis			
Negative	17	30	0.69
Positive	2	5	
Pathology			
Adenocarcinoma	11	16	
Squamous cell carcinoma	6	16	
Adenosquamous carcinoma	1	1	
Large cell carcinoma	1	0	
Small cell carcinoma	0	2	
Consistency of histological type as preceding cancer			
No	-	11	
Yes	19	24	
Recurrence after second surgery			
No	5	24	0.007
Yes	14	11	
Recurrence site‡			
lung	7	1	0.002
lymph node	5	4	0.25
pleural dissemination	3	2	0.33
intrathoracic lesion (total)	12	6	0.001
others	4	6	0.72
Survival after second surgery (median, months)	61.6	60.9	0.77

*: Pneumo: pneumonectomy, Lobe: lobectomy, Seg: segmentectomy, Wedge: wedge resection.
†: The tumor size was unknown in one patient.
‡: with overlap.

も考えられる．またたとえ気管支鏡生検が行えても，採取組織が少なく診断困難である場合や，提示した症例 1b のように，悪性診断はついても組織型が同じで鑑別には至らない症例なども存在した．今回の検討例では，同一組織型は 54 例中 43 例(79.6%)と高頻度で，しかも SPLC 症例においても 35 例中 24 例（68.6%）と頻度が高かった．Lee らも異時性肺癌の 70% 以上で 2 つの腫瘍は同一組織型であったと報告しており，[7] 肺癌では同じ組織型で多発発生しやすいことが再認識される．近年，DNA，p53，EGFR など，様々な鑑別診断の補助的方法が検討されているが，[8,9] 未だ明確な基準はない．今回の検討でも病理学的に鑑別困難な症例は少なからず経験されたが，さらにその場合には臨床経過なども参考にして，最終診断を行っている．今後は，さらに鑑別目的に適う免疫組

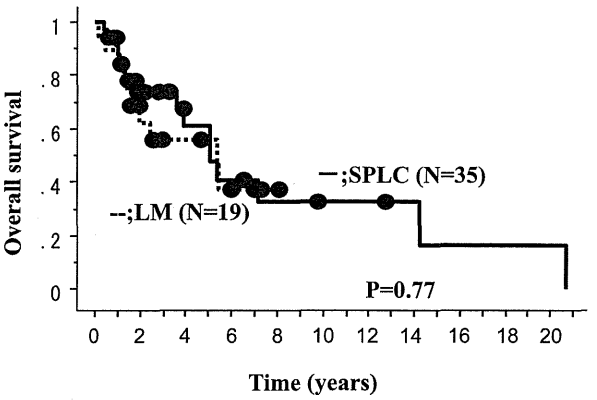

Figure 2. Kaplan-Meier curve for overall survival among the patients with solitary solid malignant lung nodules: LM or SPLC.

織染色マーカーや遺伝子マーカーの発見に期待したい.

2回目の治療方針に関し，SPLCは切除適応となる一方，LMは遠隔転移と考えて化学療法(あるいは放射線療法)も考慮される．しかし副腎，脳の孤立性遠隔転移に対する最近の報告では，切除により良好な予後が報告されるようになり，[10,11] NCCNおよびACCPガイドラインでも局所治療の有効性が明記されている．これら脳，副腎以外臓器の孤立性転移巣の局所治療の有用性については報告が少ないが，一方，部位にかかわらず転移が孤立性であれば良好な予後が期待でき，積極的な切除によりBSC，放射線療法単独，あるいは化学療法単独に比し生存率改善につながる報告もある．[12]

今回，我々は孤立性充実性肺結節に対し，SPLC，LMの如何にかかわらず切除を行った症例を対象として検討を行い，Figure 2に示すように2群間で予後に有意差を認めず(P＝0.77)，しかも2回目手術を始点とし，生存期間中央値で約5年が得られた（LM；61.6ヶ月，SPLC；60.9ヶ月，全症例；61.9ヶ月）．生存率には報告者によってばらつきがあるものの，SPLCとLMの2群間で切除後の生存率に優劣がないという報告は複数あり，我々の結果も諸家の報告に一致する．[13,14] 2回目の術式については，肺葉切除群で予後良好な傾向があるという報告もあるが，[15] 完全切除できる条件下での縮小手術を推奨する報告もある．[16] 当院では，呼吸機能温存の観点から，縮小手術を第一選択術式としているが，腫瘍径，局在位置，リンパ節転移の有無などから症例によっては根治を目指し系統的切除を行う方針としている．今回の検討では，縮小手術群と肺葉切除以上を行った系統的切除群での生存期間中央値は各々65.2ヶ月，46.8ヶ月で，縮小手術群で予後良好な傾向があった(P＝0.07)．この結果は，初回術後経過観察中，早期でLMまたはSPLCが発見された場合，縮小手術でも十分な予後が見込めることを示し，術後経過観察の重要性を示唆するものであろう．また，経過観察中に他病死した症例10例中5例が呼吸不全死であり，呼吸機能温存は多数回切除症例では特に留意すべきと考えられる．

ちなみに，当院で同時期に，肺癌術後の孤立性充実性肺結節に対し，手術以外の治療が行われた症例は13例あり，小線源療法1例を含め8例に放射線療法，3例に化学療法，1例に免疫療法，1例に分子標的療法(EGFR-TKI)が行われていた．非切除の理由は，低肺機能，合併症，低PSなど患者状態によるものが8例，CEA異常高値などで潜在的な多発再発が疑われた症例が4例，患者拒否が1例であった．13例の治療後生存期間中央値は30.1ヶ月で，切除群に比べ予後不良であった（vs 61.9ヶ月，P＝0.07）．さらに2個目の病変が初回手術と同側であった症例は13例中8例で，うち残存肺摘除術となる可能性があるため非切除となった症例が2例含まれた．残存肺摘除術は手術手技としては難度が高くリスクも伴う一方，対側肺病変の場合にも初回手術後に優占となった健側肺を切除するため，肺機能に対する評価は不可欠である．今回の検討では，切除群で予後良好であり，また2個の病変の存在側ごとに予後を比較した場合の生存期間中央値は，同側症例が62.5ヶ月，対側症例が50.0ヶ月と同等であった(P＝0.98)．よって，同側，対側にはかかわらず，術前検討を十分に行ったうえで2回目の切除を考慮してよいと考えられた．

今回の結果では，肺癌術後に発見された悪性孤立性充実性陰影を切除し得た場合，比較的良好な予後が得られた．LMかSPLCかの術前診断は困難であったが，切除症例ではLMの術後生存期間はSPLCに劣らず同等であった．このため，治療方針決定のうえでの術前鑑別診断の重要性は必ずしも高くなく，全身状態を評価のうえ，可能であれば積極的に手術適応としてよいと考えられる．ただし，手術術式については呼吸機能温存に特に留意すべきである．また，再発形式や死因に関しては両群で差を認めており，特にLM群では胸腔内再々発が多いことなどを念頭に置き，慎重な経過観察が必要と考えられる．

おわりに

1）肺癌切除後に発見された悪性孤立性充実性陰影では，多発肺癌のほか前回肺癌再発症例が含まれ，LMかSPLCかの臨床診断と病理組織学的診断の一致症例は54例中37例（68.5%）であった．

2）2回目手術術後の生存期間中央値はLMで61.6ヶ月，SPLCでは60.9ヶ月で，これら2群間に有意差を認めなかった（P＝0.77）．

3）LMとSPLCでは，2回目手術後の再発率および再発様式は異なり，LMで有意差をもって術後再発率が高く（P＝0.007），再度肺転移を多く認めた（P＝0.002）．

4）肺癌切除後に発見され，悪性が疑われた孤立性充実性陰影に対しては，積極的に手術適応と考えているが，術式については呼吸機能温存への留意が必要で，またその後の経過に関しては厳重な経過観察が必要であると考えられた．

本論文内容に関連する著者の利益相反：なし

REFERENCES

1. Sugimura H, Nichols FC, Yang P, Allen MS, Cassivi SD, Deschamps C, et al. Survival after recurrent nonsmall-cell lung cancer after complete pulmonary resection. *Ann Thorac Surg.* 2007;83:409-418.
2. Johnson BE, Cortazar P, Chute JP. Second lung cancers in patients successfully treated for lung cancer. *Semin Oncol.* 1997;24:492-499.
3. Martini N, Melamed MR. Multiple primary lung cancers. *J Thorac Cardiovasc Surg.* 1975;70:606-612.
4. Nakata M, Saeki H, Takata I, Segawa Y, Mogami H, Mandai K, et al. Focal ground-glass opacity detected by low-dose helical CT. *Chest.* 2002;121:1464-1467.
5. Nakajima R, Yokose T, Kakinuma R, Nagai K, Nishiwaki Y, Ochiai A. Localized pure ground-glass opacity on high-resolution CT: histologic characteristics. *J Comput Assist Tomogr.* 2002;26:323-329.
6. Hansell DM, Bankier AA, MacMahon H, McLoud TC, Müller NL, Remy J. Fleischner Society: glossary of terms for thoracic imaging. *Radiology.* 2008;246:697-722.
7. Lee BE, Port JL, Stiles BM, Saunders J, Paul S, Lee PC, et al. TNM stage is the most important determinant of survival in metachronous lung cancer. *Ann Thorac Surg.* 2009;88:1100-1105.
8. Sano A, Kage H, Sugimoto K, Kitagawa H, Aki N, Goto A, et al. A second-generation profiling system for quantitative methylation analysis of multiple gene promoters: application to lung cancer. *Oncogene.* 2007;26:6518-6525.
9. Gomez-Roca C, Raynaud CM, Penault-Llorca F, Mercier O, Commo F, Morat L, et al. Differential expression of biomarkers in primary non-small cell lung cancer and metastatic sites. *J Thorac Oncol.* 2009;4:1212-1220.
10. Porte H, Siat J, Guibert B, Lepimpec-Barthes F, Jancovici R, Bernard A, et al. Resection of adrenal metastases from non-small cell lung cancer: a multicenter study. *Ann Thorac Surg.* 2001;71:981-985.
11. Modi A, Vohra HA, Weeden DF. Does surgery for primary non-small cell lung cancer and cerebral metastasis have any impact on survival? *Interact Cardiovasc Thorac Surg.* 2009;8:467-473.
12. Schuchert MJ, Luketich JD. Solitary sites of metastatic disease in non-small cell lung cancer. *Curr Treat Options Oncol.* 2003;4:65-79.
13. Voltolini L, Paladini P, Luzzi L, Ghiribelli C, Di Bisceglie M, Gotti G. Iterative surgical resections for local recurrent and second primary bronchogenic carcinoma. *Eur J Cardiothorac Surg.* 2000;18:529-534.
14. 雪上晴弘，棚橋雅幸，羽田裕司，鈴木恵理子，吉井直子，丹羽　宏．再発・異時性多発癌の診断で再切除術を施行した症例の検討．胸部外科．2010;63:944-949.
15. 千田雅之，羽隅　透，星川　康，松村輔二，佐藤雅美，半田政志，他．手術適応と術式の選択　肺多発癌に対する手術適応の検討．胸部外科．2002;55:41-44.
16. Rosengart TK, Martini N, Ghosen P, Burt M. Multiple primary lung carcinomas: prognosis and treatment. *Ann Thorac Surg.* 1991;52:773-779.

Lymphatic invasion of micropapillary cancer cells is associated with a poor prognosis of pathological stage IA lung adenocarcinomas

HIROSHI HIRANO[1], HAJIME MAEDA[2], YUKIYASU TAKEUCHI[2], YOSHIYUKI SUSAKI[2], RYOZI KOBAYASHI[2], AKIO HAYASHI[2], NAOKO OSE[2], TOSHIHIKO YAMAGUCHI[3], SOICHIRO YOKOTA[3] and MASAHIDE MORI[3]

Departments of [1]Pathology, [2]Surgery and [3]Internal Medicine, Toneyama National Hospital, Toyonaka, Osaka 560-8552, Japan

Received November 7, 2013; Accepted April 16, 2014

DOI: 10.3892/ol.2014.2284

Abstract. The cancer cells of lung adenocarcinoma with a micropapillary pattern (MPP) have been found to frequently invade lymphatic vessels, and the prognosis of patients with lung adenocarcinoma with an MPP is poor. In the present study, the cancer cells of lung adenocarcinomas containing an MPP were found to express vimentin more extensively than those in lung adenocarcinoma without an MPP. The contribution of cancer cells in the MPP component to adenocarcinoma lymphatic invasion was assessed using vimentin as a marker. Vimentin expression was analyzed in the cancer cells present in each lymphatic vessel and compared with the expression of vimentin in the cancer cells in the adenocarcinomas without an MPP component. The results showed that the cancer cells in the lymphatic vessels expressed vimentin more extensively than those in the adenocarcinoma components without an MPP, suggesting that cancer cells derived from an MPP component are present in the lymphatic vessels. By contrast, the area of the MPP component in each adenocarcinoma was <25%. These findings suggest that cancer cells in MPP components have a high capacity to invade lymphatic vessels and that their high invasive capacity may be associated with a poor prognosis in patients with adenocarcinoma with an MPP component.

Introduction

Lung cancer is the leading cause of cancer-related mortality in the USA and worldwide (1). In the USA, the age-adjusted incidence and mortality rates of lung cancer (between 2004 and 2008) is 62 and 51.6 per 100,000 men and women per year, respectively, with these rates higher in men than in women (2). Of all types of lung cancer, adenocarcinoma is the most common histological subtype, accounting for ~40% of all lung cancers, and is increasing in frequency (1). Although surgery may be possible, a certain population of patients with adenocarcinomas show poor prognosis. A micropapillary pattern (MPP) in lung adenocarcinoma has been reported to be an indicator of a poor prognosis in lung adenocarcinoma (2-4). This poor prognosis has been shown to be associated with a higher frequency of lymphatic and venous invasion in lung adenocarinomas with an MPP (2-4). However, whether the cancer cells in the MPP have a role in the invasion of cancer cells into lymphatic and venous vessels has yet to be elucidated. Therefore, the present study aimed to investigate the role of cancer cells in the MPP in lymphatic and venous invasion in lung adenocarinoma using pathological stage IA lung adenocarcinoma samples.

Patients and methods

Patients. The present study included 218 patients (102 males and 116 females) with pathological stage IA lung adenocarcinoma who underwent complete resection of their tumors at Toneyama National Hospital (Toyonaka, Japan) between January 2002 and December 2010. None of the patients received neoadjuvant chemotherapy or radiotherapy. All patients underwent dissection of the bifurcation and the ipsilateral mediastinal lymph nodes, and pathological examination revealed no metastasis in these locations. Furthermore, computed tomography and magnetic resonance images showed no metastasis in any of the patients. Pathological stage was determined according to the tumor-node-metastasis classification of the International Union Against Cancer (7th edition; tumor size <3.0 cm, T1N0M0 and no pleural invasion) (5). Clinical information for each patient was obtained through reviewing medical charts. The follow-up periods ranged between 12 and 113 months (mean, 55 months). Informed consent was obtained from each patient. The present study was approved by the ethics committee of Toneyama National Hospital (approval number: 1305).

Histology. The diameters of the resected tumors were measured and the longest diameter was regarded as the tumor

Correspondence to: Dr Hiroshi Hirano, Department of Pathology, Toneyama National Hospital, 1-1, Toneyama 5-Chome, Toyonaka, Osaka 560-8552, Japan
E-mail: hihirano@toneyama.go.jp

Key words: lung adenocarcinoma, micropapillary, immunohistochemistry, pathological stage IA

diameter. The tumors were fixed in 0.01 M phosphate-buffered saline containing 10% formalin (pH 7.4) and several paraffin-embedded tumor blocks were generated from each tumor. Tumor sections (4-mm thick) were then generated from each tumor block. Sections were either used for hematoxylin and eosin staining or immunohistochemistry. Tumors were histologically classified according to the International Association for the Study of Lung Cancer (6). MPPs were identified as small tufts without a fibrovascular core, present in the alveolar spaces or in spaces encased within thin walls of connective tissues (Fig. 1), as described previously (2-4).

Immunohistochemistry. Immunohistochemical staining was performed using an avidin-streptavidin immunoperoxidase method with anti-human E-cadherin (dilution, 1:50; Novocastra, Newcastle, UK), anti-human vimentin (dilution, 1:200; Dako, Glostrup, Denmark) and anti-human D2-40 (dilution, 1:20; Dako) mouse monoclonal antibodies. Antigen retrieval was performed through incubating the deparaffinized sections in cell condition 1 solution (Ventana Medical Systems, Inc., Tucson, AZ, USA) at a low degree (the slide temperature is controlled at 36˚C). Immunohistochemical staining was then performed using an automated Benchmark system (Ventana Medical Systems) according to the manufacturer's instructions.

The grades of immunohistochemical staining for E-cadherin and vimentin were determined according to the proportion (p) of positive cells as follows: 0, p<5% positive cells; 1+, 5≤p<30% positive cells; 2+, 30≤p<70% positive cells; 3+, p≥70% positive cells.

In order to analyze the expression of vimentin in the cancer cells which had invaded into lymphatic vessels, two serial tumor sections were established and the sections were either stained for vimentin or D2-40. When cancer cells were found in a D2-40-positive lymphatic vessel in a section stained for D2-40, the grade of vimentin-positive staining of these cancer cells was analyzed in the other section stained for vimentin as described above.

Statistical analyses. Survival curves were plotted using the Kaplan-Meier method and the survival rates of the two groups were analyzed using the log-rank test. Data for more than three samples are presented as the mean ± standard error of the mean. Student's t-test was used to compare data between two groups. The differences in frequencies between two groups were analyzed using the t^2 test. All statistical analyses were performed using the Excel Statistics 2012 software package (SSRI, Tokyo, Japan) for Windows. P<0.05 was considered to indicate a statistically significant difference.

Results

Survival rates and clinicopathological chracteristics of patients with adenocarcinomas. In the present study, tumors were classified into three groups based on the proportion of the MPP area in the adenocarcinoma according to a study by Miyoshi *et al* (3). In brief, the classification was performed as follows: 0%, adenocarcinoma with no MPP component; <5%, adenocarcinoma with a focal MPP component; and >5%, adenocarcinoma with an apparent MPP component. The numbers of patients with adenocarcinoma containing no MPP component, a focal MPP component and an apparent MPP component were 171 (78.4%), 29 (13.3%) and 18 (8.3%), respectively.

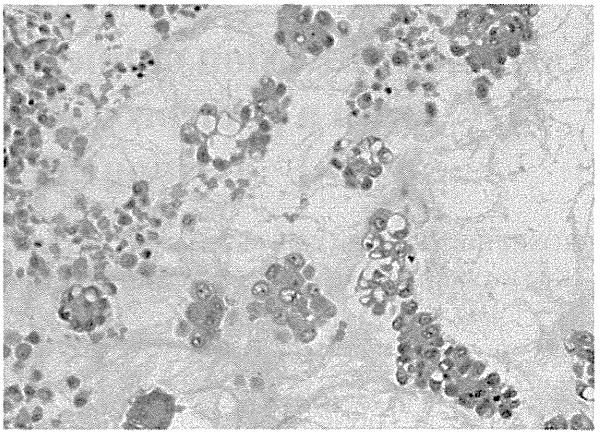

Figure 1. Micropapillary pattern in lung adenocarcinoma exhibiting papillary tufts lacking a central fibrovascular core (hematoxylin and eosin stain; magnification, x20)

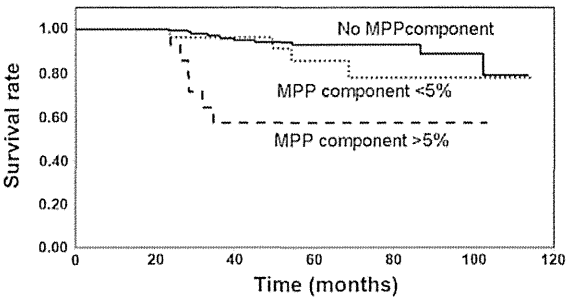

Figure 2. Survival rates of patients with adenocarcinoma containing no MPP component, those containing a focal MPP component (MPP area, <5%) and those with an apparent MPP component (MPP area, >5%). MPP, micropapillary pattern.

Fig. 2 shows the survival rates of the patients with adenocarcinoma in the different MPP groups. The survival rate of the patients with adenocarcinoma containing an apparent MPP component was significantly decreased compared with that in the patients with no MPP component or those with a focal MPP component. The survival rates of the patients with adenocarcinoma containing no MPP component and those with a focal MPP component were not significantly different.

The clinicopathological characteristics of the patients with a low survival rate (the apparent MPP component group) and those with a higher survival rate (the non- and focal MPP component groups) were compared (Table I). The patients in the apparent MPP component group were predominantly male and had a papillary predominant histology, histologically moderate differentiation and a higher frequency of cancer cell lymphatic invasion.

*ExpressionofE-cadherinandvimentin.*Epithelial-mesenchymal transition (EMT) has an important role in cancer metastasis (7). During EMT, cancer cells lose E-cadherin-mediated cell-cell adhesion and acquire characteristics of mesenchymal